Behavioral Characteristics of Graphite /AA6061 Alloy Particle-Reinforced Metal Matrix Composites

A. Chennakesava Reddy

Associate Professor, Department of Mechanical Engineering, Vasavi College of Engineering, Hyderabad, India
dr_acreddy@yahoo.com

Abstract: *In the current work, the AA6061/graphite metal matrix composites were manufactured at 10% and 30% volume fractions of graphite. The composites were subjected to mechanical and thermal loads. The microstructure of AA6061 alloy/graphite reveals the fracture of interphase and particle. As the volume fraction increases, the particle fracture is initiated at low temperature of thermal loading. The fracture of graphite particle is on account of decrease of thermal conductivity and negative thermal expansion with increase of temperature above 125°C.*

Keywords: *AA6061, graphite, spherical nanoparticle, RVE model, finite element analysis, interphase fracture.*

1. INTRODUCTION

A recent trend in composites research, especially in nanocomposites, is the use of graphite as a reinforcing material. The bond between graphite particles and metal matrix material is critical to the effectiveness of graphite as a reinforcement to enhance mechanical properties. There are interactions between the graphite and the matrix, such as the attractive van der Waals interactions. Particle composites typically contain a matrix material and inclusions. The interface between the inclusion and the matrix is a bonding surface, across which both weak and strong discontinuities occur [1]. The overall performance of a composite depends on the material properties of each phase as well as the interfacial properties between the matrix and inclusions [2]. These material and interfacial properties govern how the material fails, including such failure modes as brittle fracture, ductile rupture, debonding, yielding, and excessive deformation [3]. Composites commonly fail along the interface between the matrix and inclusion. This type of failure is called interfacial material failure and is defined as the formation of two new surfaces from a previously bonded interface between two materials. Interfacial decohesion is usually observed in composites with very low strength matrices relative to the inclusion, (i.e., ceramic inclusions in a pure aluminum matrix), while particle fracture usually occurs with a medium to high strength matrix [4]. Given the significance of interfacial damage progression on the bulk strength and toughness of composite materials, it is not surprising that one of the major research areas in composites is the modeling of bonding interfaces between phases. The interfacial zone has been modeled in a number of ways, including as a narrow region of continuum with graded properties, as an infinitely thin surface with springs, and as a cohesive zone with traction-separation relations. Micromechanical methods have been widely used for decades to study stress/strain distributions within composites, as well as the correlation between constituent properties and macro (effective) properties of composite materials [5-21].

Graphite (Gr) is a crystalline form of carbon. Graphite is the most stable form of carbon under standard conditions. Graphite has a layered, planar structure. In each layer, the carbon atoms are arranged in a honeycomb lattice with separation of 0.142 nm, and the distance between planes is 0.335 nm. Atoms in the plane are bonded covalently, with only three of the four potential bonding sites satisfied. The fourth electron is free to migrate in the plane, making graphite electrically conductive. Bonding between layers is via weak van der Waals bonds, which allows layers of graphite to be easily separated, or to slide past each other. The two known forms of graphite, alpha (hexagonal) and beta (rhombohedral), have very similar physical properties. The acoustic and thermal properties of graphite are highly anisotropic, since phonons propagate quickly along the tightly-bound planes, but are slower to travel from one plane to another. Graphite's high thermal stability and electrical conductivity facilitate its widespread use as electrodes and refractories in high temperature material processing applications. Graphite and graphite powder are valued in industrial applications for their self-lubricating and dry lubricating properties. There is a common belief that graphite's lubricating properties are solely due to the loose interlamellar coupling between sheets in the structure. Graphite (carbon) fiber and carbon nanotubes are also used in carbon fiber reinforced plastics, and in heat-resistant composites such as reinforced carbon-carbon (RCC). Commercial structures made from carbon fiber graphite composites include fishing rods, golf club shafts, bicycle frames, sports car body panels, the fuselage of the Boeing 787 Dreamliner and pool cue sticks and have been successfully employed in reinforced concrete,

In the current work, the effect of thermo-mechanical loading on the fracture in AA6061 alloy/Gr composites was predicted. The shape of Gr nanoparticle considered in this work is spherical. The periodic particle distribution was a square array and

corresponding representative volume element (RVE) is showed in figure 1. Both microscopic and micromechanics methods were employed to assess fracture in the composites.

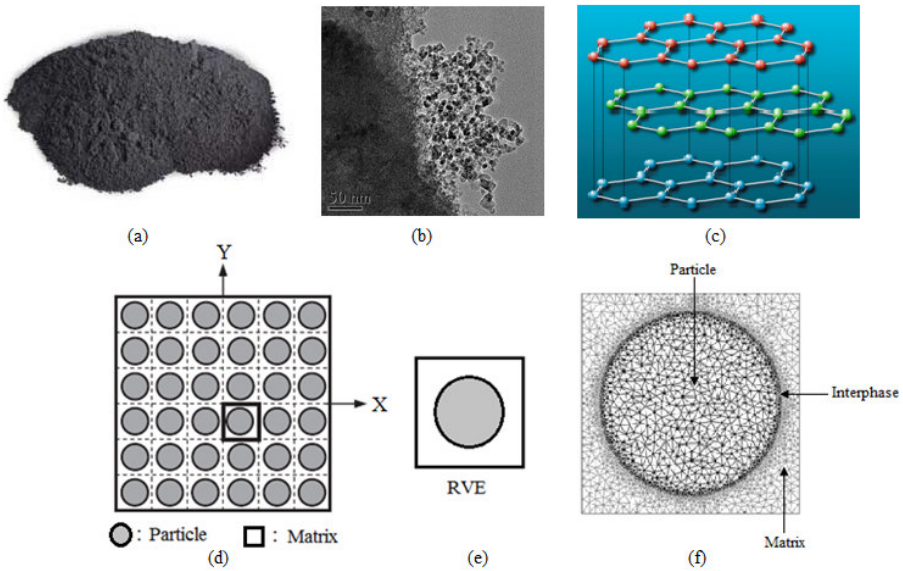

Figure 1: Graphite nanopowder (a); Gr particles (b); Crystal structure of Gr (c); Square array of particles (d); Representative volume element (e); and Discretization of RVE (f).

2. MATERIALS METHODS

The matrix material was AA6061 alloy. The reinforcement material was Gr nanoparticles of average size 100nm. The mechanical properties of materials used in the present work are given in table 1.

Table 1: Mechanical properties of AA6061 matrix and Gr nanoparticles

Property	AA6061	Gr
Density, g/cc	2.70	2.51
Elastic modulus, GPa	68.9	445.0
Coefficient of thermal expansion, 10^{-6} 1/^{o}C	23.6	5.6
Specific heat capacity, J/kg/^{o}C	896	1288
Thermal conductivity, W/m/^{o}C	167	90
Poisson's ratio	0.33	0.19

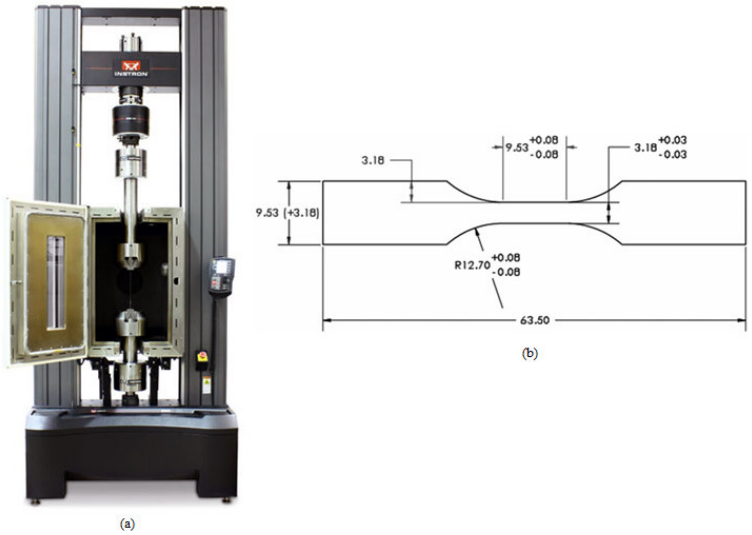

Figure 2: Tensile testing: UTM with temperature controlled chamber and (b) shape and dimensions of tensile specimen.

AA6061 alloy/Gr composites were fabricated by the stir casting process and low pressure casting technique with argon gas at 3.0 bar. The composite samples were give solution treatment and cold rolled to the predefined size of tensile specimens. The heat-treated samples were machined to get flat-rectangular specimens (figure 2) for the tensile tests. The tensile specimens were placed in the grips of a Universal Test Machine (UTM) with temperature controlled chamber at a specified grip separation and pulled until failure. The test speed was 2 mm/min. A strain gauge was used to determine elongation. In the current work, a cubical representative volume element (RVE) was implemented to analyze the tensile behavior AA6061/Gr nanoparticle composites at two (10% and 30%) volume fractions of Gr and at different temperatures. The large strain PLANE183 element was used in the matrix in all the models. In order to model the adhesion between the matrix and the particle, a CONTACT 172 element was used.

3. RESULTS AND DISCUSSION

The tested tensile specimens are shown in figure 3. Almost 50% specimens fail at centre with a little no necking formation. The optical micrograph as shown in figure 4 reveals uniform distribution of Gr particles in AA6061 alloy matrix.

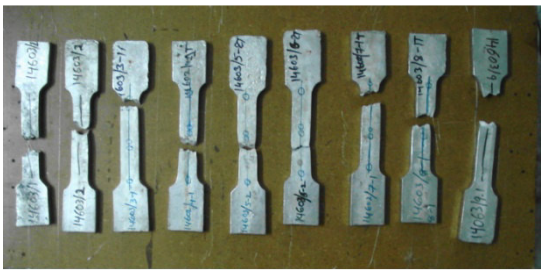

Figure 3: Tested tensile specimens.

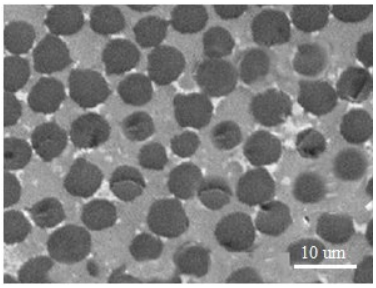

Figure 4: Microstructure showing distribution of Gr nanoparticles in AA6061 alloy matrix.

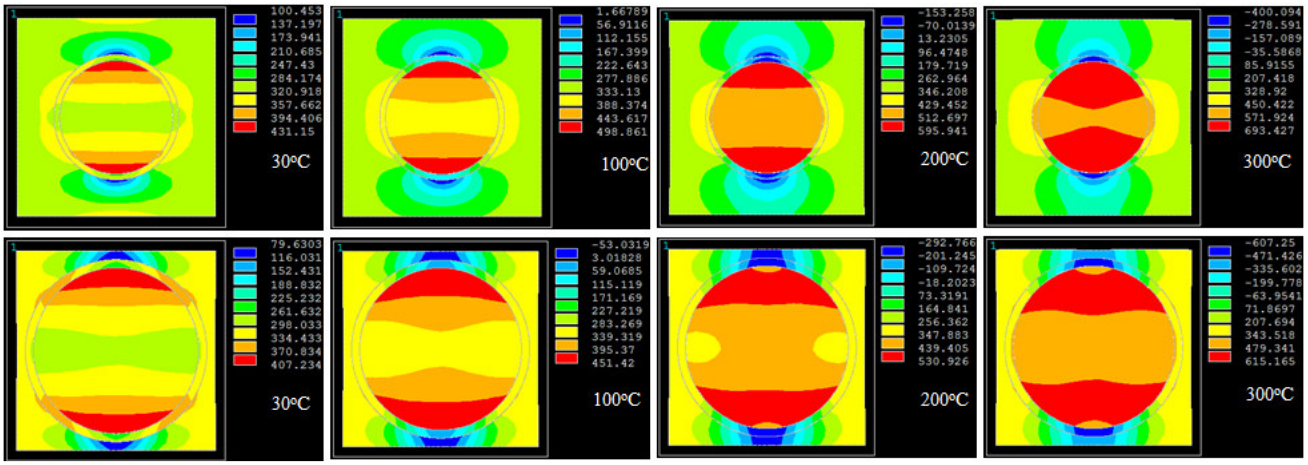

Figure 5: FEA results of tensile stress induced along load direction in the composites comprising of: (a) 10% Gr and (b) 30% Gr.

3.1 Thermo-Mechanical Behavior

Figure 5 signifies the tensile stresses induced in the AA6061/Gr composites along the load direction. The tensile stress increases with increase of temperature and it decreases with increase of volume fraction of AA6061/Gr in AA6061 alloy

matrix. It is observed that the stress induced exceeds the allowable stress as the temperature is increased. The normalized elastic modulus is shown in figure 6a. The elastic modulus is normalized with the elastic modulus of AA6061 alloy. The stiffness of the composites decreases with increase of temperature. The stiffness of AA6061 alloy/10% Gr composites is higher than that of AA6061 alloy/30% Gr composites with regard to increase of temperature. The normalized stiffness along the normal direction is lower than that along the load direction. The normalized shear modulus increases with volume fraction of Gr (figure 6b). Initially, the major Poisson's ratio decrease from 30°C to 100°C and later on it increases with temperature from 100°C to 300°C (figure 6c).

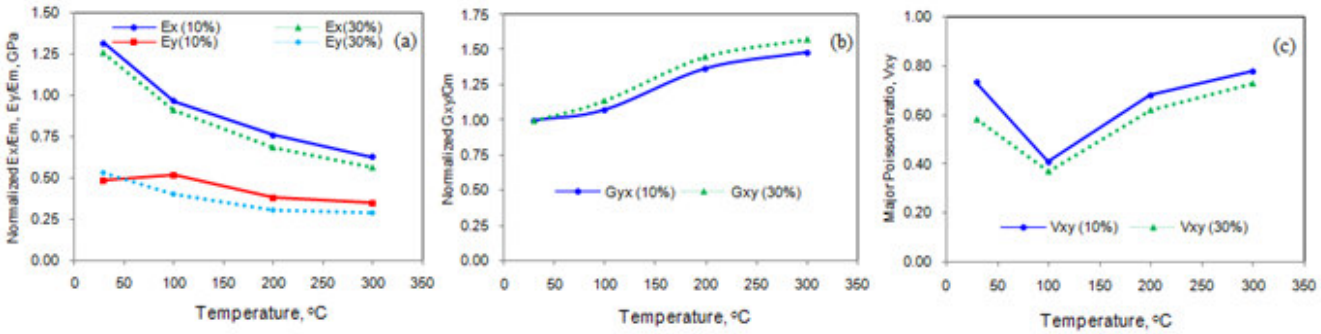

Figure 6: Effect of temperature on micromechanical properties of AA6061/ Gr composites.

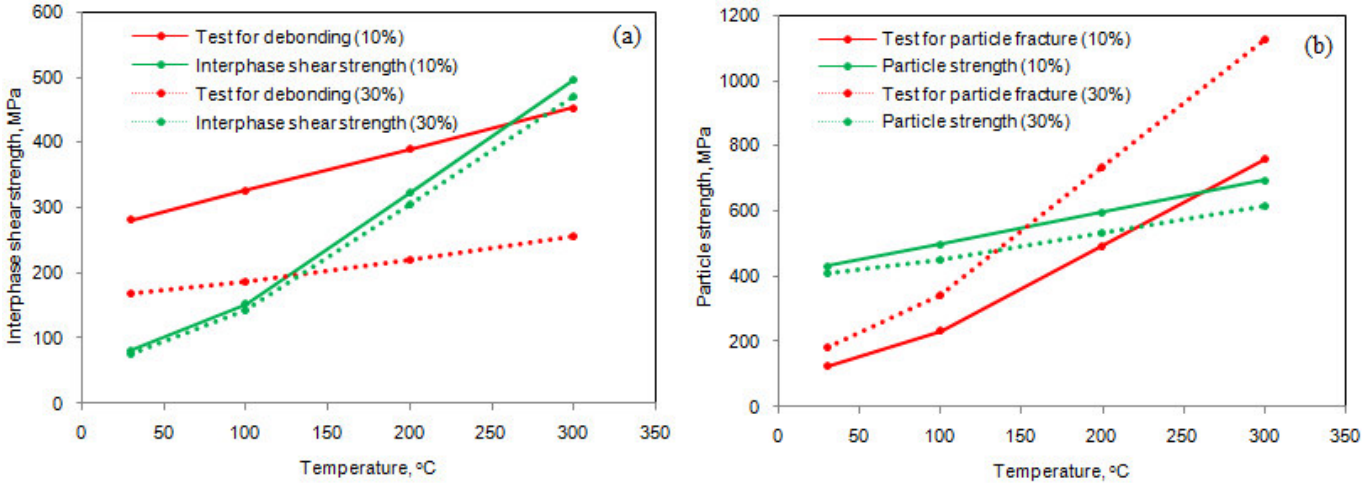

Figure 7: Criterion for interfacial debonding (a) and for particle fracture (b).

3.2 Fracture Behavior

If the particle deforms in an elastic manner (according to Hooke's law) then,

$$\tau = \frac{n}{2}\sigma_p \quad (1)$$

where σ_p is the particle stress. If particle fracture occurs when the stress in the particle reaches its ultimate tensile strength, $\sigma_{p,uts}$, then setting the boundary condition at

$$\sigma_p = \sigma_{p,\,uts} \quad (2)$$

The relationship between the strength of the particle and the interfacial shear stress is such that if

$$\sigma_{P,uts} < \frac{2\tau}{n} \quad (3)$$

Then the particle will fracture. From the figure 7b, it is observed that the Gr nanoparticle was not fractured as the condition in Eq. (3) is not satisfied below 250°C for the composites AA6061/10% Gr composites and below 125°C for the composites AA6061/30% Gr, respectively. The particle fracture occures above 250°C for the composites AA6061/10% Gr composites and above 125°C for the composites AA6061/30% Gr, respectively. This is due to CTE and stiffness mismatches between Gr nanoparticles and AA6061 alloy matrix. For the interfacial debonding/yielding to occur, the interfacial shear stress reaches its shear strength:

$$\tau = \tau_{max} \quad (4)$$

For particle/matrix interfacial debonding can occur if the following condition is satisfied:

$$\tau_{max} < \frac{n\sigma_p}{2} \quad (5)$$

It is observed from figure 7a that the interphase debonding occurs between Gr nanoparticle and AA6061 alloy matrix as the condition in Eq.(5) is satisfied below 250°C for the composites AA6061/10% Gr composites and below 125°C for the composites AA6061/30% Gr, respectively. The debonding phenomenon is high in the composites comprising of 30% Gr.

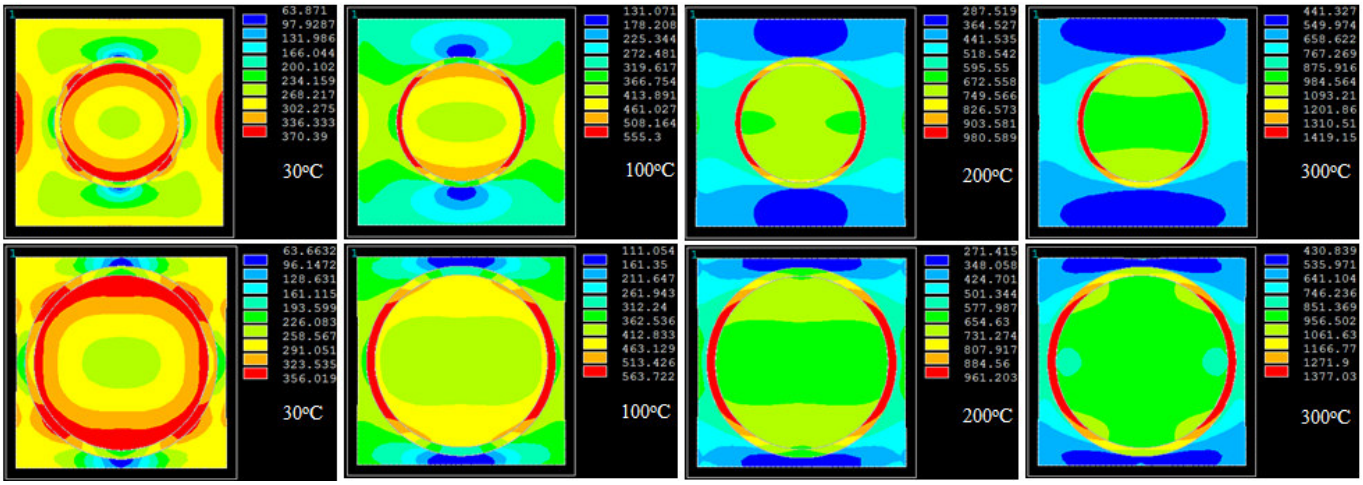

Figure 8: Images of von Mises stresses obtained from FEA: (a) AA6061/10% Gr and (b) AA6061/30% Gr composites.

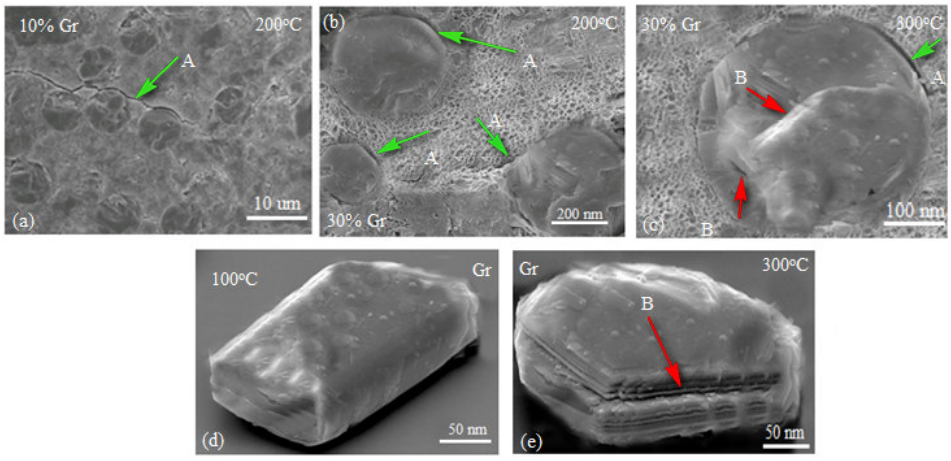

Figure 9: SEM images showing interphase debonding (A) and particle fracture (B).

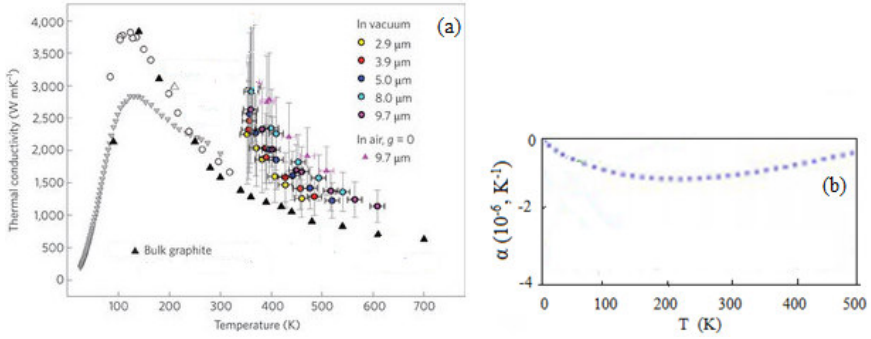

Figure 10: Thermal properties of graphite.

The von Mises stress induced at the interface are higher than that induced in the nanoparticle (figure 8). Hence, the interfacial interphase fracture was occurred between the particle and the matrix. The particle fracture is initiated in AA6061/30% Gr

composites at 125°C of thermal loading and in AA6061/ 10% Gr composites at 250°C of thermal loading, respectively, due to thermal shock. The microstructure shown in figure 9 confirms the occurrence of interphase and particle fractures in the composites. The interphase debonding increases with increase of temperature. As observed from figure 10, the thermal conductivity of graphite increases from 0°C to 150°C and it decreases later on with increase of temperature. The graphite demonstrates negative thermal expansion with increase of temperature. These may be the reasons for the fracture of graphite particles in AA6061 alloy matrix with increase of temperature above 125°C. The fracture of graphite is clearly visible as shown in figure 10e when heated graphite particles in a muffle furnace at 300°C.

4. CONCLUSION

The microstructure of AA6061 alloy/ Gr composites reveals the uniform distribution of Gr nanoparticles in the matrix. The shear stress is high at the interface resulting to interphase debonding in AA6061/ Gr composites. The particle fracture has occurred above 250°C in AA6061/ 10% Gr composites and above 125°C of thermal loading in AA6061/ 30% Gr composites, respectively. The microstructures obtained from the experimental samples confirm the fracture of interphase between the Gr particles and AA6061 alloy matrix and particle fracture. The fracture of graphite particle is due to decrease of thermal conductivity and negative thermal expansion with increase of temperature.

REFERENCES

1. K. K. Chawla, Composite Materials Science and Engineering, Springer Science Business, New York, 1998.
2. A. Needleman, A continuum model of void nucleation by inclusion debonding, Journal of Applied Mechanics, 54, 1987, pp. 525–531.
3. V. Tvergaard, Effect of fiber debonding in a whisker-reinforced metal, Materials Sciience and Engineering, 125, 1990, pp. 203–213.
4. A. F. Whitehouse, T. W. Clyne, Cavity formation during tensile straining of particulate and short fiber metal-matrix composites, Acta Metallurgica et Materialia, 41, 1993, pp.1701–1711.
5. A. Chennakesava Reddy, Effect of Particle Loading on Microealstic Behavior and interfacial Tractions of Boron Carbide/AA4015 Alloy Metal Matrix Composites, 1st International Conference on Composite Materials and Characterization, Bangalore, March 1997, pp. 176-179.
6. A. Chennakesava Reddy, Reckoning of Micro-stresses and interfacial Tractions in Titanium Boride/AA2024 Alloy Metal Matrix Composites, 1st International Conference on Composite Materials and Characterization, Bangalore, March 1997, pp. 195-197.
7. A. Chennakesava Reddy, Evaluation of Debonding and Dislocation Occurrences in Rhombus Silicon Nitride Particulate/AA4015 Alloy Metal Matrix Composites, 1st National Conference on Modern Materials and Manufacturing, Pune, India, 19-20 December 1997, pp. 278-282,.
8. A. Chennakesava Reddy, Interfacial Debonding Analysis in Terms of Interfacial Tractions for Titanium Boride/AA3003 Alloy Metal Matrix Composites, 1st National Conference on Modern Materials and Manufacturing , Pune, 19-20 December, 1997.
9. A. Chennakesava Reddy, Assessment of Debonding and Particulate Fracture Occurrences in Circular Silicon Nitride Particulate/AA5050 Alloy Metal Matrix Composites , National Conference on Materials and Manufacturing Processes, Hyderabad, India, 27-28 February 1998, pp. 104-109.
10. A. Chennakesava Reddy, Local Stress Differential for Particulate Fracture in AA2024/Titanium Carbide Nanoparticulate Metal Matrix Composites, National Conference on Materials and Manufacturing Processes, Hyderabad, India, 27-28 February 1998, pp. 127-131.
11. A. Chennakesava Reddy, Micromechanical Modelling of Interfacial Debonding in AA1100/Graphite Nanoparticulate Reinforced Metal Matrix Composites, 2nd International Conference on Composite Materials and Characterization, Nagpur, India, 9-10 April 1999, pp. 249-253.
12. A. Chennakesava Reddy, Cohesive Zone Finite Element Analysis to Envisage Interface Debonding in AA7020/Titanium Oxide Nanoparticulate Metal Matrix Composites, 2nd International Conference on Composite Materials and Characterization, Nagpur, India, 9-10 April 1999, pp. 204-209.
13. B. Kotiveera Chari, A. Chennakesava Reddy, Debonding Microprocess and interfacial strength in ZrC Nanoparticle-Filled AA1100 Alloy Matrix Composites using RVE approach, 2nd National Conference on Materials and Manufacturing Processes, Hyderabad, India, 10-11 March 2000, pp. 104-109.
14. A. Chennakesava Reddy, Micromechanical and fracture behaviors of Ellipsoidal Graphite Reinforced AA2024 Alloy Matrix Composites, 2nd National Conference on Materials and Manufacturing Processes, Hyderabad, India, 10-11 March 2000, pp. 96-103.

15. S. Sundara Rajan, A. Chennakesava Reddy, Micromechanical Modeling of Interfacial Debonding in Silicon Dioxide/AA3003 Alloy Particle-Reinforced Metal Matrix Composites, 2nd National Conference on Materials and Manufacturing Processes, Hyderabad, India, 10-11 March 2000, pp. 110-115.
16. S. Sundara Rajan, A. Chennakesava Reddy, Role of Volume Fraction of Reinforcement on Interfacial Debonding and Matrix Fracture in Titanium Carbide/AA4015 Alloy Particle-Reinforced Metal Matrix Composites, 2nd National Conference on Materials and Manufacturing Processes, Hyderabad, India, 10-11 March 2000, 116-120.
17. A. Chennakesava Reddy, Constitutive Behavior of AA5050/MgO Metal Matrix Composites with Interface Debonding: the Finite Element Method for Uniaxial Tension, 2nd National Conference on Materials and Manufacturing Processes, Hyderabad, India, 10-11 March 2000, pp. 121-127.
18. B. Kotiveera Chari, A. Chennakesava Reddy, Interfacial Debonding of Boron Nitride Nanoparticle Reinforced 6061 Aluminum Alloy Matrix Composites, 2nd National Conference on Materials and Manufacturing Processes, Hyderabad, India, 10-11 March 2000, pp. 128-133.
19. P. M. Jebaraj, A. Chennakesava Reddy, Simulation and Microstructural Characterization of Zirconia/AA7020 Alloy Particle-Reinforced Metal Matrix Composites, 2nd National Conference on Materials and Manufacturing Processes, Hyderabad, India, 10-11 March 2000, pp. 134-140.
20. P. M. Jebaraj, A. Chennakesava Reddy, Continuum Micromechanical modeling for Interfacial Debonding of TiN/AA8090 Alloy Particulate Composites, 2nd National Conference on Materials and Manufacturing Processes, Hyderabad, India, 10-11 March 2000, pp. 141-145.
21. Hill, R., 1963, “Elastic Properties of Reinforced Solids: Some Theoretical Principles”, Engineering Journal of the Mechanics and Physics of Solids, Pergamon Press Ltd. Great Britain, 11, pp. 357-372.